Bulk Spinodal Decomposition Studied by Atomic Force Microscopy and Light Scattering

J. T. Cabral and J. S. Higgins*

Department of Chemical Engineering, Imperial College, London SW7 2BY, UK

T. C. B. McLeish

IRC in Polymer Science and Technology, Department of Physics and Astronomy, University of Leeds, Leeds LS2 9JT, UK

S. Strausser and S. N. Magonov*

Digital Instruments/Veeco Metrology Group, 112, Robin Hill Rd., Santa Barbara, California 93117

Received October 13, 2000; Revised Manuscript Received February 1, 2001

ABSTRACT: We report the first observation of bulk spinodal decomposition in polymer blends using atomic force microscopy (AFM). The fracture of a phase-separated thick film of tetramethyl bisphenol A polycarbonate (TMPC) and polystyrene (PS) is shown to induce a surface roughness that is resolvable by AFM. The resulting topography reproduces the spinodal morphology and is analyzed quantitatively. We investigate simultaneously the surfaces and bulk of the TMPC/PS films, a blend known to exhibit surface-directed spinodal decomposition. The structure factors obtained from a 2D-FFT of "bulk" AFM images and from time-resolved light scattering (LS) do not coincide—this is discussed in terms of the 2D (AFM) and 3D (LS) analysis involved. We finally compute general expressions relating 2D and 3D structure factors for a number of structures relevant to phase separation phenomena.

I. Introduction

Partially miscible polymer blends quenched inside the unstable region of the phase diagram undergo spinodal decomposition (SD). Isotropic composition fluctuations develop with selectively amplified wavelengths. Initially, the amplitudes of these fluctuations grow exponentially with time, characterized by a growth rate, $R(q)$, which is parabolic in the square of the wavenumber, q ($q = 2\pi/\Lambda$, where Λ is the wavelength of a composition fluctuation); the distribution has a time-independent maximum at q_m and a cutoff, due to the energy cost of sharp interfaces, at $q_c = 2^{1/2}q_m$.[1] The process gives rise to the well-known three-dimensional bicontinuous morphology.

Subsequently, coarsening of phase-separated domains takes place, driven by chemical potential gradients at interfaces. Initial coarsening is slow, dominated by chain diffusion, and the characteristic domain size increases with time, following $t^{1/3}$—the so-called evaporation−condensation mechanism. It accelerates at later times, for which the domain shape relaxes due to hydrodynamic flow, exhibiting a t^1 dependence.[2] Some doubt has recently been cast on whether it is possible to further attain, in practice, the inertial asymptote (characterized by $t^{2/3}$) predicted by Furukawa,[2b] in the case of polymer blends.[2c] The initial length scale of these concentration fluctuations (which can, to a certain extent, be tuned by the temperature quench depth inside the spinodal) falls in the submicron scale.

Phase separation of polymer blends can be probed using a number of experimental techniques. These may be classified, on the basis of the analysis employed, as real- or reciprocal-space techniques. The former includes optical microscopy, transmission and scanning electron microscopy, and atomic force microscopy; the scattering techniques—light, neutron, or X-ray—fall in the latter. Real-space experiments are qualitatively more informative but require the use of Fourier analysis to obtain further quantitative insight; this can, however, be misleading if a limited spatial region is probed.

A scattering experiment measures directly the structure factor, $S(q)$, which correlates concentration fluctuations, providing therefore a convenient quantitative tool to study phase separation:

$$S(\mathbf{q},t) = \langle \phi(\mathbf{q},t)\, \phi(-\mathbf{q},t) \rangle = S(q,0) \exp(2R(q)t) \quad (1)$$

where $\phi(\mathbf{q},t)$ is the Fourier transform of a spatial composition fluctuation at time t, $\phi(\mathbf{r},t)$, and $q = 4\pi n/\lambda \sin(\theta/2)$ its wavenumber, θ being the scattering angle and n the refractive index of the medium. The last equality in (1) holds for the early stages for which a growth rate, $R(q)$, can be defined as the amplification factor of fluctuations of wavenumber q.

The choice of a suitable technique depends on the length scale window of interest. Small-angle neutron or X-ray scattering (SANS, SAXS) provide adequate spatial resolution for studying the earliest stages of phase separation,[3] typically covering $0.01 \leq q \leq 0.2$ nm^{-1}. The resolution provided by TEM and SEM can also probe such fine structures. After further coarsening (or for very shallow quenches), light scattering (covering about $0.001 \leq q \leq 0.02$ nm^{-1}) and then optical microscopy (OM) become the relevant techniques. The experimental contrast of SANS or SAXS arises respectively from differences in scattering length density (typically requiring deuteration of one component) or electronic density between the compounds. Electron microscopy requires the microtoming and selective staining of samples. For LS and OM studies, a significant refractive index difference is necessary to resolve phase separation. In fact, contrast is a most relevant issue for all the aforementioned techniques since the initial compo-

10.1021/ma0017743 CCC: $20.00
Published on Web 04/26/2001

sition profile is smooth, and even the equilibrium composition of the resulting phases may be very similar (as for near-critical shallow quenches).

Phase separation (and competing surface wetting) of miscible polymer blends in thin films, under various interfacial geometries and segregation regimes, has recently attracted much theoretical and experimental attention.[4−16] The confinement in a film and component segregation to the interfaces have been shown to have a profound effect in both spinodal decomposition (SD) and nucleation and growth (N&G)—not only in the kinetics but also in the nature of the phase separation. In the vicinity of an interface (within about 1 μm) to which one component is preferentially attracted, the isotropy of structure is lost, and "surface-directed" SD occurs.[4,6,9] Composition fluctuations are therefore no longer randomly oriented but grow perpendicularly to the surface, originating a lamellar type of ordering close to the interface, which fades away toward the bulk. This process is suppressed[8] for films even thinner than the characteristic wavelength of the fluctuations—in so-called "ultrathin" films[8,10−13] (with thicknesses below about 0.25 μm). Phase separation occurs then parallel to the surface and, due to surface tension modulations of the phases, gives rise to surface undulations.[11−13] Accordingly, domain coarsening was also found to progress with modified kinetics[5,7,11] and possibly even "pinning" in a metastable long-lasting morphology.

AFM has played an important role in elucidating the aforementioned phase separation and wetting phenomena in thin films.[7,10,12−16] It is particularly suited to study phase separation and wetting phenomena in "utrathin" films, probing directly the induced surface roughening.[12−15] Otherwise, in immiscible blends,[17−20] a selective dissolution of components is usually required. This allows one to obtain composition−depth profiles but involves the risk of creating artifacts, such as washing away dispersed (nonsoluble) phases.

Atomic force microscopy, which was introduced more than 10 years ago,[21] had attracted initial attention of scientists by its capabilities to generate topographic surface maps with unique resolution and to visualize atomic-scale lattices of crystalline samples. By learning more about force interactions between a sharp tip and a sample surface, which are used for probing surfaces in AFM, and about the ways to control them, considerable progress in AFM applications to polymer materials has been achieved.[22] The spectrum of AFM applications to polymers is not limited by high-resolution imaging of their surfaces. Surface studies of heterogeneous polymer systems such as block copolymers and polymer blends at elevated tip−sample forces allow compositional mapping of these materials,[22] which is primarily based on differences of mechanical properties of individual components. Further, in examination of polymer materials with a rubbery-like topmost layer an AFM probe can penetrate underneath this layer and visualize polymer organization at different depths.[23] This shows that AFM is not only a surface technique. To prepare bulk polymer samples for AFM, one can use a microtome, which is routinely applied for transmission electron microscopy (TEM). However, unlike TEM samples, which need to be cut thin and of uniform thickness (about 50−100 nm), there are no such thickness requirements for AFM samples.[18,24−26c]

In this work, in further exploration of AFM capabilities for polymer characterization, we have examined spinodal decomposition in thick (50−100 μm) films of a well-known polymer blend exhibiting lower critical solution temperature (LCST) phase behavior: tetramethyl bisphenol A polycarbonate and polystyrene.[27] Though surface phase separation patterns developing in *thin* films of polymer blends have already been analyzed with AFM, this is the first *bulk* phase separation study. The experimental procedure is described in section II. In section IIIA, we present AFM images obtained from both the cross section and the surfaces of thick phase-separated films of TMPC/PS, annealed inside the unstable spinodal region for varying times. We show that the topography of the cross-sectioned film reflects SD patterns identical to those obtained by conventional optical polarization microscopy. Furthermore, we study the same samples by time-resolved light scattering (section IIIB). Because of the higher spatial resolution of AFM, the SD morphology can be detected during earlier stages of the process than with LS. In section IIIC, we obtain structure factors as a function of time from both methods and realize that the results are not identical. The differences are, at least in part, explainable by the different dimensionality of the measurements. With these ideas in mind, we then derive quantitative relationships between two-dimensional (2D) and three-dimensional (3D) structure factors (as for AFM and LS, respectively) for a variety of structures, in particular for the early and late stages of phase separation.

II. Experimental Section

A. Materials. Tetramethyl bisphenol A polycarbonate (TMPC) and polystyrene (PS) form a partially miscible blend exhibiting a lower critical solution temperature (LCST) phase behavior.[27] Blends of TMPC (M_W = 54 000 g/mol, PDI = 3.5, T_g = 197 °C,[29] Bayer) and PS (M_W = 225 000 g/mol, PDI = 2.2, T_g = 102 °C, BP Chemicals) of near-critical composition (50:50 weight fraction) were utilized in this study. TMPC/PS films were prepared by solution casting from tetrahydrofuran (10% w/v) onto 100 μm thick glass slides. Films were dried for 4 weeks under vacuum (at increasing temperatures, up to the blend glass transition temperature, T_g) to remove traces of solvent, resulting in thickness of 50−100 μm.

Films were first allowed to equilibrate at a temperature just below the phase boundary (230 °C). Spinodal decomposition was then initiated by a temperature jump to 245 °C (~5 °C inside the spinodal[27]). This thermal treatment was done on a hot stage while performing time-resolved LS.

B. Light Scattering. We have employed a homemade apparatus, consisting of a 5 mW He−Ne laser, a hot stage (temperature control 0.2 K), and an array of photodiodes covering an angular range of 5−67°. Samples were isothermally annealed in the unstable region for different time intervals from 50 to 1000 s and then quenched below the blend's glass transition temperature. The samples were then reanalyzed to verify that no further coarsening had occurred during the temperature quench. These same films were examined using AFM and optical microscopy.

C. Atomic Force Microscopy. The phase-separated films were first peeled from the thin glass substrate. The free-standing films were then cross-sectioned at room temperature with a MicroStar ultramicrotome using a diamond knife (both products of Micro Star Technologies, TX). Top and bottom surfaces of the films and their cross sections were then examined with optical microscopy (OM) and AFM. We have also prepared cross sections of some films by fracture at room temperature. For a few cases, some regions of the fracture surfaces were flat enough to obtain high-quality AFM images. However, this procedure is less consistent than the microtoming. Note that, at room temperature, both TMPC and PS (and therefore any mixed composition) are well below the glass transition.

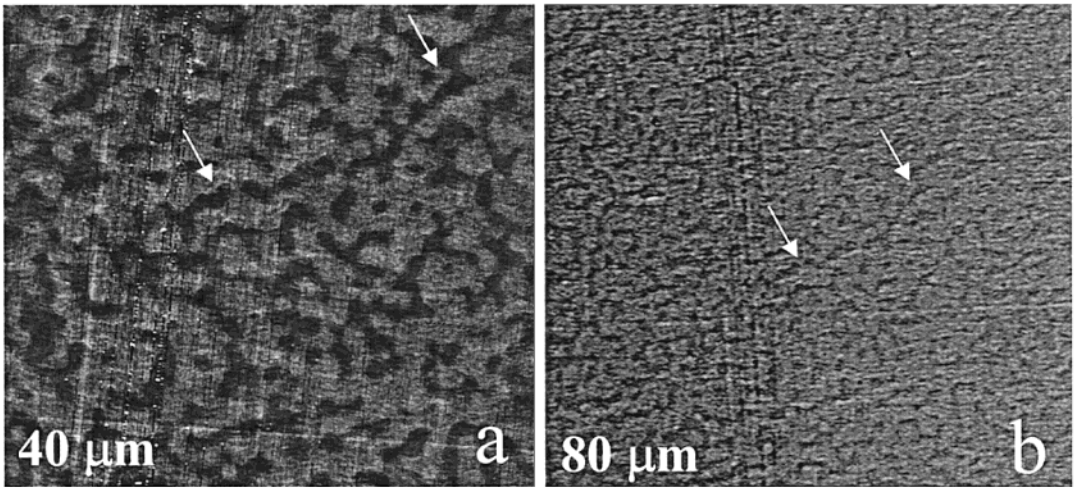

Figure 1. Spinodal decomposition in a thick film of TMPC/PS 50:50 blend annealed for 1000 s at 245 °C. (a) AFM height image of the microtomed surface of the bulk film (40 × 40 μm^2 scan) and (b) corresponding optical micrograph (80 × 80 μm^2 scan). The arrows define the same region in both images.

Optical polarization micrographs in reflectance mode were first obtained with a Nikon optical microscope equipped with a digital camera and an Optronics module (Optronics, Santa Barbara, CA) for comparison purposes.

AFM measurements were performed at ambient conditions with a scanning probe microscope MultiMode Nanoscope IIIA (Digital Instruments, Santa Barbara, CA). Experiments were conducted in tapping mode with commercial Si probes (stiffness ~ 40 N/m, resonant frequency 160−170 kHz). In all experiments, height and phase images were recorded simultaneously, yet for the reasons discussed below, our analysis was based mostly on height images. The amplitude of the free-oscillating probe A_0 was chosen in the 10−20 nm range and the set-point amplitude A_{sp} in the $0.5-0.8A_0$ range. Variations of the amplitudes are essential for imaging soft materials at different tip-force levels. Low tip-force conditions (small A_0 and A_{sp} close to A_0) are most suitable for a gentle and high-resolution imaging of top surface features. Imaging at high tip force or hard tapping (high A_0 and $A_{sp} \sim 0.4-0.5A_0$) is recommended for compositional imaging of heterogeneous polymer samples.[22c] For the analysis of AFM height images we have applied 2D fast Fourier transforms (FFT) to obtain the power spectra of phase-separated structures observed at different stages of SD.

III. Results and Discussion

A. Atomic Force Microscopy. The cross-sectioned phase-separated films (both fractured and microtomed) were found to exhibit a surface topography resolved by AFM. In an initial stage of our research, we have therefore investigated the origin of such topography by comparing an optical polarization micrograph and AFM height images obtained at the same location of a cross section of TMPC/PS films annealed for 1000 s. This relatively long time was chosen because it corresponds to a coarsening regime, for which composition profiles are well-defined. The patterns observed in Figure 1a,b are identical: the arrows point to the similar shaped dark regions. This implies that the composition differences (of the TMPC- or PS-rich phases) are responsible both for the polarization contrast and for the topography of the microtomed surface. In other words, the observed topography mirrors the spinodal structure. The surface roughness is small but resolvable by AFM, namely from about 1 to 4 nm (rms), increasing with annealing time. Phase separation patterns identical, although less neat, to those seen on the microtomed surfaces were observed in AFM height images of a fractured surface (Figure 2b). This is due to a much higher surface roughness, which can go up to several tens of nanometers. There is, however, a difference in the apparent volume fraction of the phases (discussed below).

The observed topography is thought to arise from differences in plastic deformation between the phase-separated domains when the sample is fractured. Thermoplastics may exhibit a variety of fracture behaviors, depending on temperature and strain rate.[28] These can range from pure brittle (low temperature) to ductile fracture (approaching the glass transition), for which nonreversible deformation occurs. Even though both PS and TMPC are brittle polymers (and well below T_g at room temperature), the differential deformation between phases is shown to be resolvable by AFM. This fracture-induced height contrast should depend on the fracture temperature and is likely to vanish in the cryogenic limit. Fracture caused by microtoming or simple fracture produce rather similar topographies, the first being best suited for AFM studies due to an overall surface flatness. We cannot, at present, unambiguously identify the PS-rich and TMPC-rich domains. Since the morphology results from a shallow quench of a near-critical mixture, their compositions are rather similar. Selective dissolution of one phase, a common procedure in immiscible blends, is therefore not possible. We will resolve this issue employing off-critical mixtures, which yield phases of clearly different volume fractions.

AFM phase images were recorded simultaneously with height images and generally reveal consistent morphologies. Phase contrast should arise from the induced topography and/or from differences in mechanical properties of the phase-separated domains. However, they are less pronounced than the topographic patterns (especially at smaller annealing times) even when imaging was performed at elevated tip force, which typically leads to enhanced phase image contrast for heterogeneous polymer systems. The poorer contrast of phase images, relative to the topographic images, may be related to the phase separation process itself. Once a homogeneous blend is quenched inside the spinodal, the (growing) amplitudes of the composition fluctuations are small. Therefore, even when the spinodal structure is already defined, the composition profiles are not sharp. These initially smooth profiles therefore may not

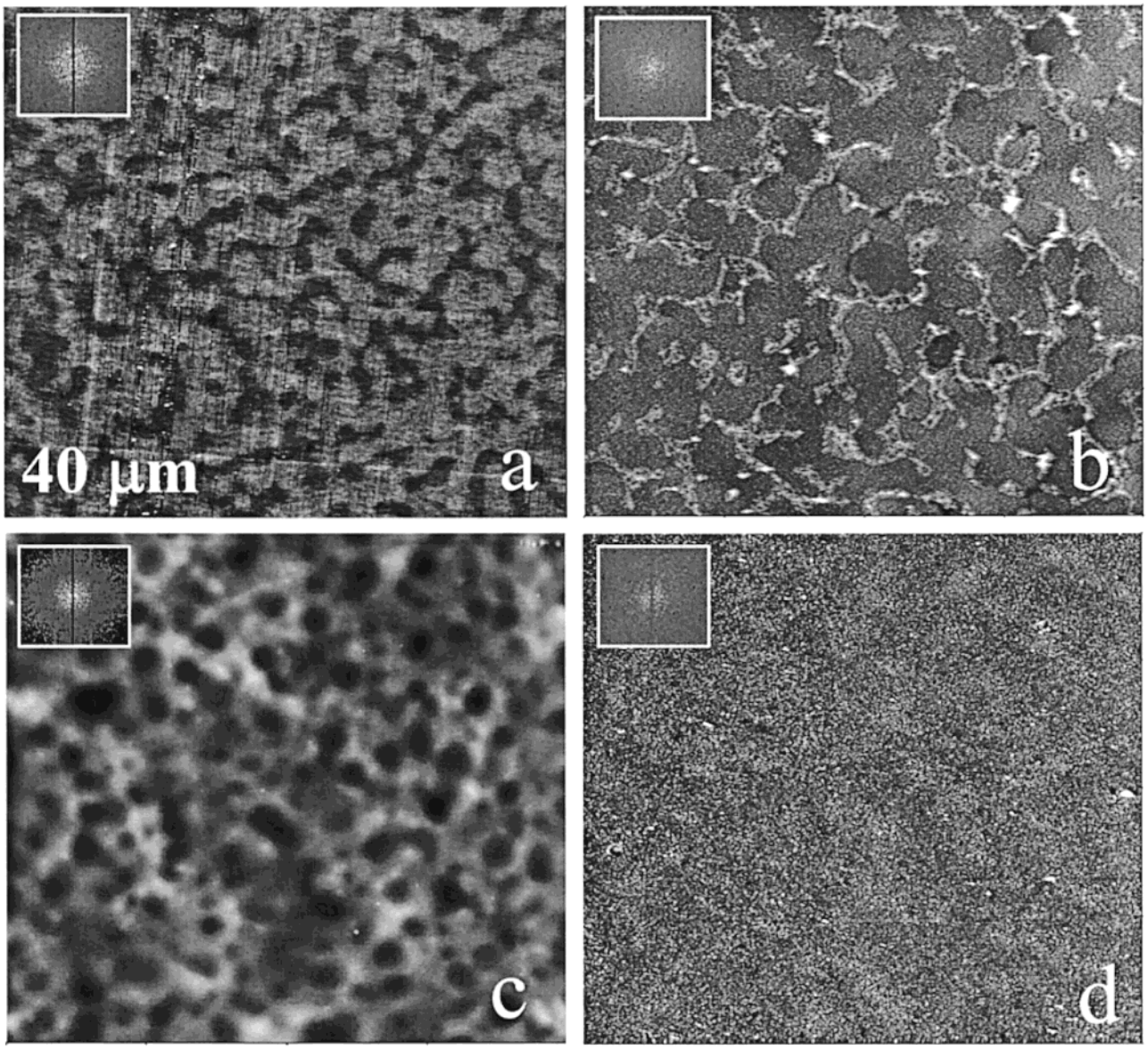

Figure 2. AFM height images ($40 \times 40\ \mu m^2$) of a phase-separated TMPC/PS 50:50 film after 1000 s at 245 °C of (a) microtomed surface (as shown in Figure 1a) and (b) fractured surface. Surface height images of (c) the top surface (air−interface) and of (d) the bottom surface, in contact with glass substrate. Insets show the power spectrum obtained after a 2D-FFT of the images.

provide substantial phase image contrast; the similar densities of TMPC and PS (respectively 1.084 and 1.05 g/cm^3) should also contribute to the reduced contrast. This difficulty is overcome during coarsening, at later stages of phase separation. In contrast, microtoming samples with a diamond knife reveals topographies which are resolvable with AFM height imaging at earlier stages of SD.

The top (air−interface) and bottom (in contact with the glass substrate) surfaces of the thick TMPC/PS films were also examined with AFM. The topography of the surfaces, shown in Figure 2c,d, is rather different from the one observed in the bulk (microtomed or fractured) and can be rationalized in terms of an asymmetric segregation of the compounds during spinodal decomposition. Surface-directed SD has been observed in near-critical TMPC/PSd (deuterated PS) blends using time-of-flight forward recoil spectrometry (FRES).[9] This was the first observation of this kind on an LCST blend. The isotropy of the bulk spinodal morphology is broken due to a differential attraction of the species to the surfaces. Films of various thicknesses (1−0.1 μm) were cast onto oxidized silicon wafers and annealed in the unstable region resulting in asymmetric segregation: PSd was found to be attracted to the air−interface while TMPC to the silicon oxide surface. Symmetric segregation of PSd was obtained by coating the Si substrate with a self-assembled monolayer of octadecyltrichlorosilane (OTS).

The topography of the top and bottom surfaces, presented in Figure 2c,d, is consistent with an expected segregation of PS to the air−interface and of TMPC to the glass substrate. Each surface, air and glass, is enriched with the component with respective lower surface energy. The surface roughening observed at the top and bottom, induced by an interplay of wetting and phase separation, differs therefore from the bulk morphology. As expected, the air−interface roughness is substantially larger than that of the (immobile) glass interface. Wetting is incomplete due to the rather short annealing times. However, the image of the top surface is compatible with an expected formation of channels, connecting the wetting layer to the bulk, "feeding" the surface with the segregated compound.

The composition waves extend from the surface into the bulk, where isotropic phase separation dominates (Figure 1a), driven solely by thermal fluctuations. A quantitative study of the surface images will be reported separately. This investigation can, in principle, be extended to a systematic depth study of microtomed surfaces (from the surface to the bulk), yielding the real-space morphology of surface-directed SD. Evidences of such phenomena have, up to now, been provided by FRES[4,6,9] (or nuclear reaction analysis, NRA) which probes a surface average of the components volume fraction as a function of depth.

The coarsening of the phase-separated structure was further investigated with AFM. Samples were isothermally annealed (at 245 °C) for different times, then quenched at room temperature, and microtomed as described above. Figure 3 presents the time evolution of the bulk spinodal morphology as seen by AFM topography of the microtomed films. The 2D height images were then fast Fourier transformed to provide quantitative information about the characteristic length scale of phase separation (inset in Figure 3).

Microtoming did not introduce substantial artifacts on the surface topography, with the exception of the first image (Figure 3a) obtained at the earliest time, which exhibits some degree of anisotropy. These experimental results establish AFM as a quantitative tool for bulk phase separation studies of polymer blends.

B. Light Scattering. Time-resolved LS is conventionally used for phase separation studies and was therefore employed for comparison purposes with our AFM study. The LS contrast is provided by the difference in refractive index between species ($n = 1.546$ and 1.591 respectively for TMPC and PS). The structure factor of the phase-separating blend as a function of time is represented in Figure 4. The time evolution of the dominant length scale of SD is shown in the insert: q_m, the wavenumber corresponding to the largest fluctuation amplitude, is represented as a function of time and shown to exhibit a t^{-1} dependence. This is characteristic of a symmetric blend undergoing coarsening due to hydrodynamic flow, relaxing domain shapes, as expected for such a relatively deep quench inside the spinodal.[2] The use of rather thick films compared to the thin anisotropic surface layers ensures that the overall scattering patterns are largely determined by bulk SD.

It is noticeable that AFM resolves the structure even at the earliest time (50 s), at which LS detects no sign of phase separation—the length scale is out of the accessible q range and the refractive index contrast small. The spatial resolution provided by our AFM study, of the orders of few tens of nanometers, and the spatial range covered, encompassing the relevant 0.1−100 μm range, are therefore particularly well suited to probe phase separation phenomena. These are significant improvements over OM and even LS, which bridge the gap to microscopic scattering techniques, such as SANS.

C. Comparison of AFM and LS Measurements. Figure 5 presents the structure factors obtained by radial average of the 2D-FFT height AFM images (referred to as "power spectra") at several quench times; these are represented as a function of $q = 2\pi/\Lambda$. The wavenumbers corresponding to the AFM structure factor maxima, q_m, are quantitatively compared to those extracted from LS (inset in Figure 4) and depicted in the inset of Figure 5. As can be seen, while exhibiting a similar time dependence, there is an offset (of the order of 1.5) between the two sets of data. The AFM structure factors shown were extracted from 40 μm^2 scans. The results were, however, cross-checked with scans ranging from 10×10 to 80×80 μm^2 to avoid artifacts arising from a limited observation region.

There are well-known limitations of microscopy techniques employed in phase separation phenomena arising when (a) the focal depth is too large compared to the examined structure or (b) when the precipitate size is smaller than the lateral resolution. The first implies that the image is not truly 2D, while the second means that those structures are not observable or may contribute as background noise. These effects are largely reduced by the use of laser scanning confocal microscopy (LSCM),[26] which reduces the focal depth down to ~500 nm and of TEM, given the use of thin specimens (50−100 nm). However, these issues should not be relevant to our AFM work since the generated topography is reduced to a genuine 2D image.

The source of AFM height contrast, as discussed above, is interpreted as arising from a different deformation of the phases under fracture. This could bias the results if, for example, one phase would appear larger than its actual size—this is, in fact, observable when comparing images of a simple fracture (Figure 2b) to that of a microtomed specimen (Figure 2a), where the volume fractions of the phases (expected to be equal) appear asymmetric in the former. However, the actual periodicity of the structure (i.e., the position of the maxima) should remain constant. In other words, even if the shape of the structure factor may change, the position of the maximum should not.

In the following, we put forward geometrical considerations that, under some circumstances, predict the observed offset. We first recall that the AFM structure factor is obtained by Fourier transforming an image of a cross section (2D) of the spinodal structure (3D). On the contrary, the LS spectra appear naturally as 3D Fourier transforms of the structure.

In fact, an apparent larger structure in 2D arises in a straightforward way from the way random directions of waves in 3D project onto a plane. Each plane wave arising from a fixed **q** in 3D is a lamellar structure in space with spacing $2\pi/q$, but the only 2D slices through this structure that share the same spacing are those for which **q** lies in the plane of the cut itself. All other planes acquire a projected lamellar spacing of $2\pi/(q \sin(\theta))$, where θ is the angle between **q** and the plane normal. So a "powder average" of waves at fixed q and projected onto a spatial plane will give rise to finite contributions to the 2D scattering function at all lower q (but no higher). Here we summarize the findings of calculations given in the Appendix. We show there that the form of the 2D scattering function $S_2(q)$ produced in this way from a 3D function $S_3(q) = \delta(q - q_0)$ is

$$S_2(q) = \Theta(q_0 - q)\frac{q}{q_0\sqrt{q_0^2 - q^2}} \qquad (2)$$

This function clearly still has a maximum (in fact, an integrable singularity) at $q = q_0$, but the *average* value of q in the 2D pattern is $\pi q_0/4$. This means that a broad scattering function in 3D will typically have its peak shifted to smaller q. Moreover, the broader the 3D distribution, the larger will be the shift in q seen in the 2D slice. For example, a simple Gaussian function with

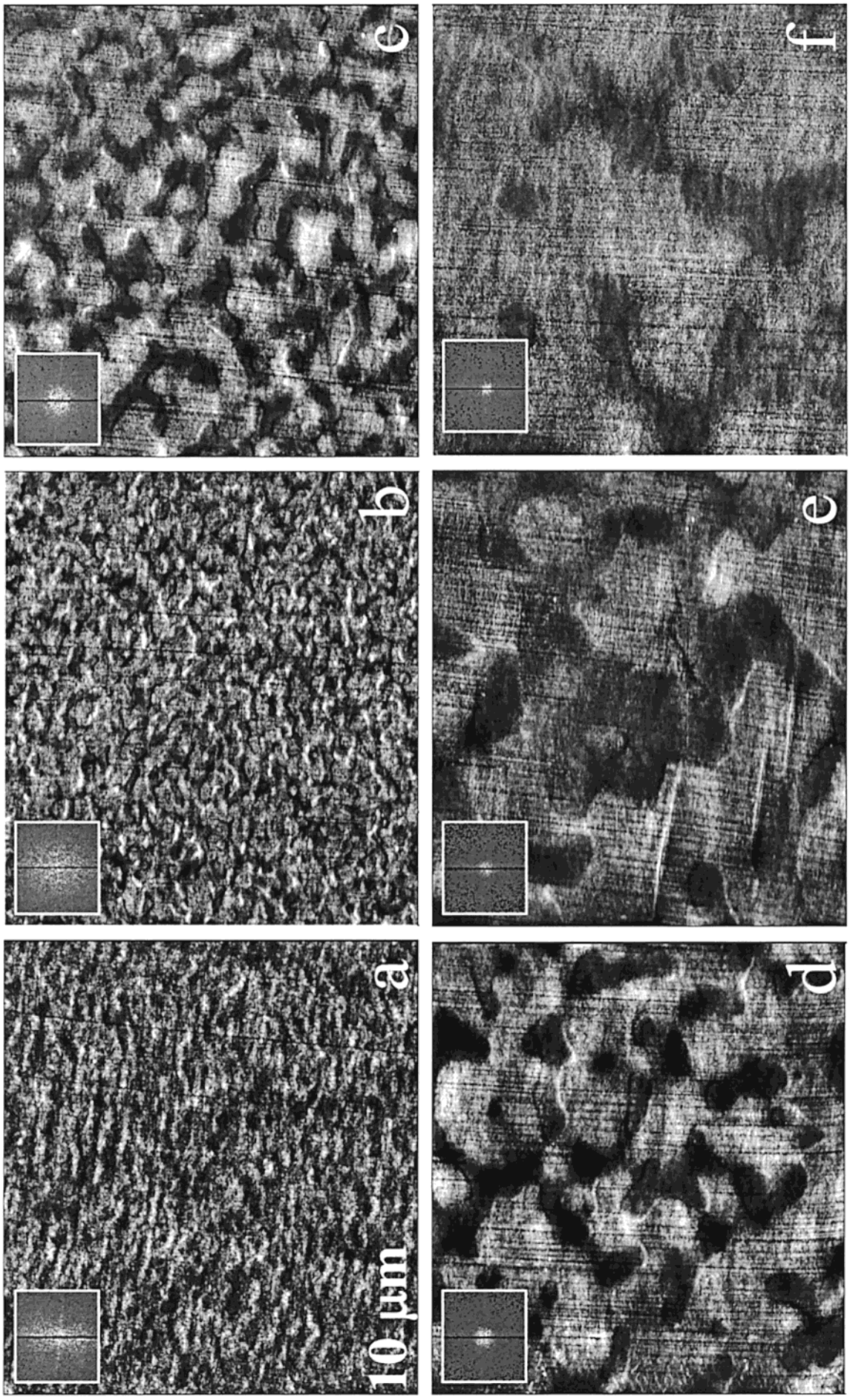

Figure 3. Bulk spinodal decomposition kinetics of TMPC/PS 50:50 studied by AFM topography. Microtomed surfaces of samples annealed (245 °C) at various times: (a) 50, (b) 100, (c) 300, (d) 500, (e) 700, and (f) 1000 s. The insets are 2D-FFT of the AFM images based on the $10 \times 10\ \mu m^2$ scans.

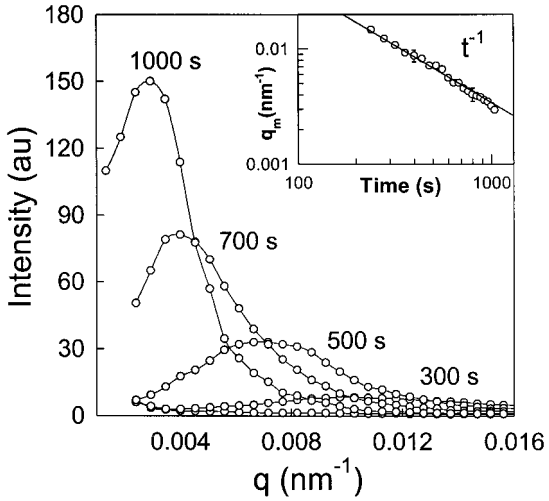

Figure 4. Structure factor at several times of a TMPC/PS 50:50 mixture undergoing spinodal decomposition at 245 °C (lines are guides to the eyes). The inset shows a double-logarithmic plot of the time evolution of q_m (wavenumber corresponding to peak maximum) indicating the hydrodynamic nature of the coarsening process (charaterized by a t^1 dependence).

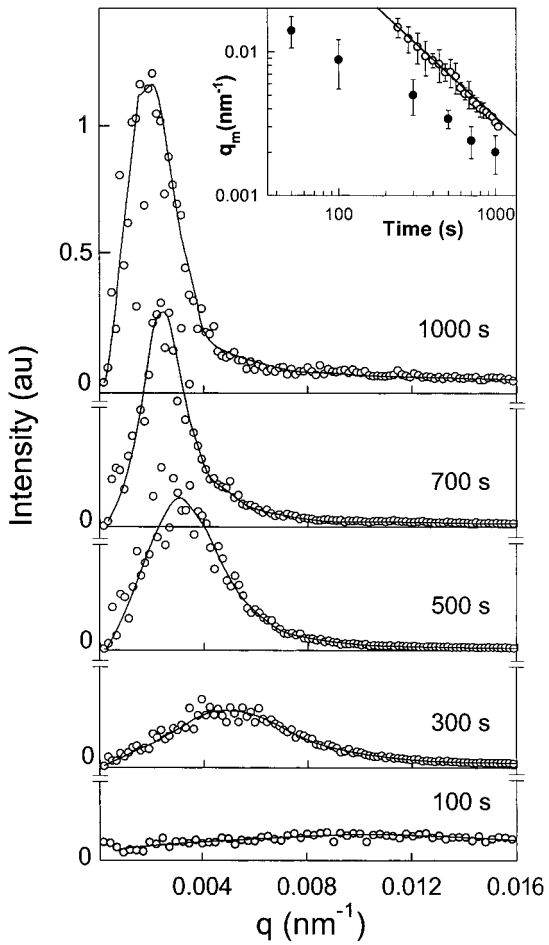

Figure 5. Power spectra (in relative units) obtained from the radial average of the 2D-FFT AFM topographies (based on 40 × 40 μm^2 scans), represented as a function of $q = 2\pi/\Lambda$ (for the same q range as in Figure 4). The inset is a comparison of LS and AFM data: the maximum fluctuation amplitude wavenumber, q_m, obtained from both methods (●, AFM data; ○, LS data) is represented as a function of time.

a maximum at q_0 and variance of σ^2 has a 2D pattern with a maximum at approximately $q_0(1 - \sigma^2/4q_0^2)$.

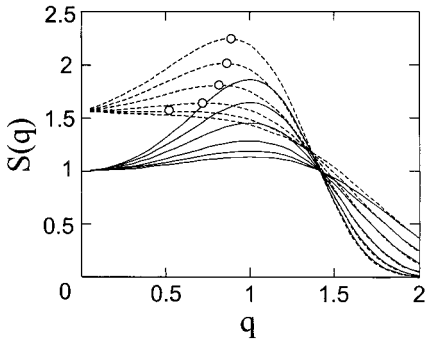

Figure 6. Structure factors predicted by early-stage Cahn−Hilliard linear theory (for dimensionless times $t = 0.5$, 0.7, 1, 1.5, 2, and 2.5). The solid line is the 3D structure factor, $S_3(q)$, and the dashed line its 2D counterpart, $S_2(q)$. The markers indicate the maxima of $S_2(q)$, of abscissa q_m(2D).

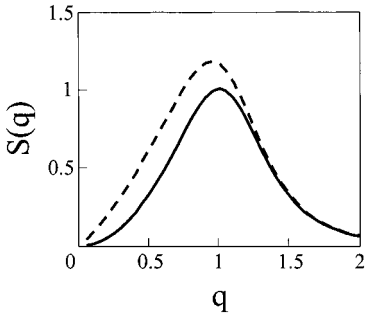

Figure 7. Late stage spinodal decomposition: the solid line is the 3D scattering function (after Furukawa[2b]). The dashed line is the calculated 2D structure factor (see text).

In Figure 6, we give representative 3D (continuous line) and their corresponding 2D (dashed line) scattering functions predicted by early-time Cahn−Hilliard (linear) theory. The functional form for the 3D intensities is written as $S_3(q) = \exp[t(q^2/2 - q^4/4)]$ and shown for dimensionless times $t = 0.5$, 0.7, 1, 1.5, 2, and 2.5. At the earliest time the maximum in the 2D spectrum is actually at $q = 0$. The markers record the approach of the maximum q in 2D to the 3D value as the peak sharpens.

It is interesting to note that this effect, although not commented upon, is visible in the early simulations of spinodal decomposition by Cahn:[1b] the wavelength observable in the 2D slices is larger than the imposed Λ of the simulated 3D structure.

A functional form for the late stage scattering function predicted by Furukawa is $S_3(q) = 4q^2/(3 + q^8)$.[2b] In Figure 7, we show the dimensionless 3D and 2D scattering functions calculated from this result. In this case, the shift in the maximum is only about 5%, but this is less than any of the shifts calculated for the exponentially growing linear response functions above, so is consistent with the observation of converging values of q_m seen in our data. There is no exact quantitative agreement with C−H predictions. Indeed, the clear coarsening of the experimental structures beyond 100 s indicates that the experiment is well beyond the linear regime there, yet the ratios of maximum q take values predicted only in the linear regime (compare the insert of Figure 5 with Figure 6). This is unsurprising to some extent, since experimental scattering functions are typically broader than the idealized theoretical ones, which will always lead to larger shifts to q_m on projection into 2D. However, a reverse calculation of the 2D structure factor based on

the experimental $S(q)$ obtained by LS does not yield such a large q_m offset as observed experimentally. We shall report again on this issue in the near future.

There have been studies of phase separation combining real- and reciprocal-space experimental techniques, with the advent of LSCM. Hashimoto and collaborators[26] have succeeded in reconstructing the 3D spinodal structure of UCST blends by superposing successive layers of LSCM scans. The obtained morphologies were either 3D-Fourier transformed and then compared to LS structure factors[26a] or 2D-FFT and compared with both TEM and LS structure factors.[26c] In the second case, liable to exhibit the currently reported effects, only TEM measurements were available at the earlier stages, and consistent agreement among the sets of data was obtained.

IV. Summary

Spinodal decomposition in bulk polymer blends was investigated for the first time using atomic force microscopy. Using optical microscopy and light scattering, we demonstrate that the topography is directly related to the spinodal morphology. We propose AFM as an interesting alternative technique for inspection of bulk phase separation in amorphous polymer blends, enjoying an enhanced resolution and larger experimental spatial window over conventionally used LS. The experimental procedure is, however, demanding. It requires annealing, quenching, and microtoming the samples (not permitting the real-time, fast acquisition rate of LS), but nevertheless simpler than for TEM.

We have further compared quantitatively the structure factors derived from AFM and LS based on the same samples. The periodicity of the structure obtained by AFM appears to be larger than what is expected by LS. We have shown that, on geometric grounds, this is to be expected in the early stages of SD. However, the magnitude of the observed shift, in the coarsening regime, is larger than the expected theoretically.

The fracture of a phase-separated sample is shown to induce a surface topography, which we interpret as stemming from a differential plastic deformation of the phases. The height should therefore (a) depend on the difference in ductility of the composite phases and (b) should vary with temperature (as fracture goes from brittle to ductile). The range of applicability of the method is currently under investigation.

The system chosen for this study was TMPC/PS, which is known to undergo surface-directed spinodal decomposition, induced by differential compound attraction to certain substrates. We have shown preliminary data on real-space observations of, for the first time, both the surface and the bulk structure. These phenomena are usually investigated by FRES or NRA, which produce average profiles as a function of depth. A reconstruction of AFM images of successively microtomed films at increasing depth would provide the 3D, very high-resolution, real-space morphology from the surface into the bulk.

Acknowledgment. We are grateful to Prof. A. J. Kinloch for useful discussions on fracture of polymer composites. J.S.H. thanks UCSB for sabbatical support and introduction to AFM. J.T.C. acknowledges the financial support from Fundação para a Ciência e Tecnologia, Portugal.

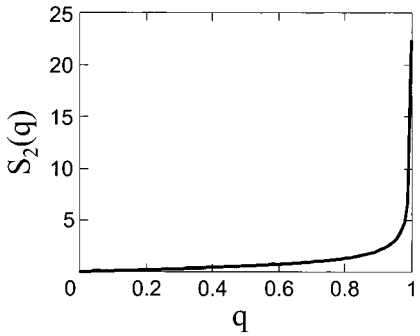

Figure 8. Plot of eq 4, $S_2(q)$ as a function of the wavenumber for $q_0 = 1$.

Appendix. Comparison of 3D and 2D Structure Factors

Let a single harmonic wave of wavenumber $\mathbf{q}_0$ intersect with a flat surface at an angle θ to the surface. Then the wavenumber of the wave projected onto the surface is $q = q_0 \sin \theta$. The projected wave always has a longer wavelength than the original wave. Now suppose that the 3D waves impinge on the 2D cut from all directions on the shell at $q = q_0$ isotropically. The 2D projected result will also be isotropic in the plane but contain amplitude for waves of all values of q from 0 to q_0. The amount of solid angle contributing to the intensity from angle θ also varies as sin θ, so we may write the total intensity in the 2D plane as

$$S_2(q) = \int_0^{\pi} d\theta \sin \theta \, \delta(q - q_0 \sin \theta) \tag{3}$$

The integral is readily done with the result

$$S_2(q) = \Theta(q_0 - q) \frac{q}{q_0 \sqrt{q_0^2 - q^2}} \tag{4}$$

where Θ is the Heaviside step function. We plot this (Green's) function for $q_0 = 1$ in Figure 8. So for a single wavenumber, the peak in the 2D scattering is still at q_0. Only for broad distributions in q does the convolution produce large shifts in the apparent peak position. For an arbitrary isotropic intensity distribution in three dimensions $S_3(q)$, the resulting projection onto 2D is simply a convolution of this function with the source:

$$S_2(q) = \int_q^{\infty} S_3(q_0) \frac{q}{q_0 \sqrt{q_0^2 - q^2}} \, dq_0 \tag{5}$$

This is the result used to calculate the mappings from 3D to 2D power spectra in the discussion above. The result for narrow Gaussians is obtained by a steepest-descents approximation on the resulting integral.

References and Notes

(1) First proposed by: (a) Cahn, J. W.; Hilliard, J. E. *J. Chem. Phys.* **1958**, *28*, 258; **1959**, *31*, 688. (b) Cahn, J. W. *J. Chem. Phys.* **1965**, *42*, 93. Extended to polymer blends by: (c) de Gennes, P.-G. *J. Chem. Phys.* **1980**, *72*, 4756. (d) Pincus, P. *J. Chem. Phys.* **1981**, *75*, 1996. (e) Binder, K. *J. Chem. Phys.* **1983**, *79*, 6387.

(2) Late stages of spinodal decomposition. (a) Siggia, E. D. *Phys. Rev. A* **1979**, *20*, 595. (b) Furukawa, H. *Adv. Phys.* **1985**, *34*, 703. (c) Kendon, V. M.; Desplat, J.-C.; Blandon, P.; Cates, M. E. *Phys. Rev. Lett.* **1999**, *83*, 576. In the case of polymer blends: private communication. (d) For a recent review, see: Doi, M. In *Theoretical Challenges in the Dynamics of Complex*

Fluids; McLeish, T. C. B., Ed.; NATO ASI Series, Series E: Applied Sciences; Kluwer Academic: Dordrecht, 1997; Vol. 339, p 293.
(3) Higgins, J. S.; Benoît, H. C. *Polymers and Neutron Scattering*; Clarendon Press: Oxford, 1994; Chapter 8. Higgins, J. S.; Fruitwala, H.; Tomlins, P. E. *Macromolecules* **1989**, *22*, 3674.
(4) Jones, R. A. L.; Norton, L. J.; Kramer, E. J.; Bates, F. S.; Wiltzius, P. *Phys. Rev. Lett.* **1991**, *66*, 1326.
(5) Wiltzius, P.; Cumming, A. *Phys. Rev. Lett.* **1991**, *66*, 3000.
(6) Krausch, G.; Dai, C. A.; Kramer, E. J.; Bates, F. S. *Phys. Rev. Lett.* **1993**, *71*, 3669.
(7) Saraf, R. F. *Macromolecules* **1993**, *26*, 3623.
(8) Krausch, G.; Dai, C. A.; Kramer, E. J.; Bates, F. S. *Ber. Bunsen-Ges. Phys. Chem.* **1994**, *98*, 446.
(9) Kim, E.; Krausch, G.; Kramer, E. J.; Osby, J. O. *Macromolecules* **1994**, *27*, 5927.
(10) Tanaka, K.; Yoon, J.-S.; Takahara, A.; Kajiyama, T. *Macromolecules* **1995**, *28*, 934.
(11) Sung, L.; Karim, A.; Douglas, J. F.; Han, C. C. *Phys. Rev. Lett.* **1996**, *76*, 4368.
(12) Karim, A.; Slawecki, T. M.; Kumar, S. K.; Douglas, J. F.; Satija, S. K.; Han, C. C.; Russell, T. P.; Liu, Y.; Overney, R.; Sokolov, J.; Rafailovich, M. H. *Macromolecules* **1998**, *31*, 857.
(13) Ermi, B. D.; Karim, A.; Douglas, J. F. *J. Polym. Sci., Polym. Phys. Ed.* **1998**, *36*, 191.
(14) Heier, J.; Kramer, E. J.; Revesz, P.; Battistig, G.; Bates, F. S. *Macromolecules* **1999**, *32*, 3758.
(15) Newby, B. Z.; Composto, R. J. *Macromolecules* **2000**, *33*, 3274.
(16) Patterned-directed SD: Böltau, M.; Walheim, S.; Mlynek, J.; Krausch, G.; Steiner, U. *Nature* (*London*) **1998**, *3391*, 877. Nisato, G.; Ermi, B. D.; Douglas, J. F.; Karim, A. *Macromolecules* **1999**, *32*, 2356.
(17) Slep, D.; Asselta, J.; Rafailovich, M. H.; Sokolov, J.; Winesett, D. A.; Smith, A. P.; Ade, H.; Strzhemechny, Y.; Schwarz, S. A.; Sauer, B. B. *Langmuir* **1998**, *14*, 4860.
(18) Thomann, Y.; Suhm, J.; Thomann, R.; Bar, G.; Maier, R.-D.; Mulhaupt, R. *Macromolecules* **1998**, *31*, 5441.
(19) Ade, H.; Winesett, D. A.; Smith, A. P.; Qu, S.; Ge, S.; Sokolov, J.; Rafailovich, M. *Europhys. Lett.* **1999**, *45*, 526.
(20) Walheim, S.; Boltau, M.; Mlynek, J.; Krausch, G.; Steiner, U. *Macromolecules* **1997**, *30*, 4995. Walheim, S.; Ramstein, M.; Steiner, U. *Langmuir* **1999**, *15*, 4828.
(21) Binnig, G.; Quate, C. F.; Gerber, C. *Phys. Rev. Lett.* **1986**, *56*, 930.
(22) For recent reviews, see: (a) Magonov, S. N.; Reneker, D. *Annu. Rev. Mater. Sci.* **1997**, *27*, 175. (b) *Scanning Probe Microscopy of Polymers;* Ratner, B., Tsukruk, V. V., Eds.; ACS Symposium Series; American Chemical Society: Washington, DC, 1998; p 694. (c) Magonov, S. N. In *Encyclopedia of Analytical Chemistry*; Meyers, R. A., Ed.; John Wiley & Sons Ltd.: Chichester, 2000; p 7432.
(23) Magonov, S. N.; Cleveland, J.; Elings, V.; Denley, R.; Whangbo, M.-H. *Surf. Sci.* **1997**, *85*, 201.
(24) Galuska, A. A.; Poulter, R. R.; McElrath, K. O. *Surf. Interface Anal.* **1997**, *25*, 418.
(25) Pfau, A.; Janke, A.; Heckmann, W. *Surf. Interface Anal.* **1999**, *27*, 410.
(26) (a) Jinnai, H.; Nishikawa, Y.; Koga, T.; Hashimoto, T. *Macromolecules* **1995**, *28*, 4782. (b) Ribbe, A. E.; Hashimoto, T.; Jinnai, H. *J. Mater. Sci.* **1996**, *31*, 5837. (c) Ribbe, A. E.; Hashimoto, T. *Macromolecules* **1997**, *30*, 3999.
(27) (a) Guo, W.; Higgins, J. S. *Polymer* **1990**, *31*, 699. (b) Kim, E.; Kramer, E. J.; Osby, J. O.; Walsh, D. J. *J. Polym. Sci., Polym. Phys. Ed.* **1995**, *33*, 467. (c) Merfeld, G. D.; Paul, D. R. *Polymer* **2000**, *41*, 649. (d) Cabral, J. T.; Gerard, H.; Higgins, J. S. *J. Chem. Phys.*, to be submitted.
(28) Kinloch, A. J.; Young, R. J. *Fracture Behaviour in Polymers*; Chapman and Hall: London, 1983.
(29) M_W and PDI are the weight-average molecular weight and polydispersity index, respectively. T_g stands for glass transition temperature (measured by differential scanning calorimetry (DSC) at 10 K/min).

MA0017743